

Multivariable Robust Control of a Simulated Hybrid Solid Oxide Fuel Cell Gas Turbine Plant

Alex Tsai

*Dissertation Submitted to the College of
Engineering and Mineral Resources at
West Virginia University*

In partial fulfillment of the requirements for the degree of

*Doctor of Philosophy
In
Mechanical Engineering*

*Larry Banta, PhD Chair
Muhammad Choudhry, PhD
Mario Perhinschi, PhD
Natalia Schmid, PhD
David Tucker, PhD*

*Department of Mechanical Engineering
2007*

Copyright 2007 Alex Tsai

UMI Number: 3300918



UMI Microform 3300918

Copyright 2008 by ProQuest Information and Learning Company.
All rights reserved. This microform edition is protected against
unauthorized copying under Title 17, United States Code.

ProQuest Information and Learning Company
300 North Zeeb Road
P.O. Box 1346
Ann Arbor, MI 48106-1346

Abstract

Multivariable Robust Control of a Simulated Hybrid Solid Oxide Fuel Cell Gas Turbine Plant

Alex Tsai

This work presents a systematic approach to the multivariable robust control of a hybrid fuel cell gas turbine plant. The hybrid configuration under investigation built by the National Energy Technology Laboratory comprises a physical simulation of a 300kW fuel cell coupled to a 120kW auxiliary power unit single spool gas turbine. The public facility provides for the testing and simulation of different fuel cell models that in turn help identify the key difficulties encountered in the transient operation of such systems. An empirical model of the built facility comprising a simulated fuel cell cathode volume and balance of plant components is derived via frequency response data. Through the modulation of various airflow bypass valves within the hybrid configuration, Bode plots are used to derive key input/output interactions in transfer function format. A multivariate system is then built from individual transfer functions, creating a matrix that serves as the nominal plant in an H_{∞} robust control algorithm. The controller's main objective is to track and maintain hybrid operational constraints in the fuel cell's cathode airflow, and the turbo machinery states of temperature and speed, under transient disturbances. This algorithm is then tested on a Simulink/MatLab platform for various perturbations of load and fuel cell heat effluence.

As a complementary tool to the aforementioned empirical plant, a nonlinear analytical model faithful to the existing process and instrumentation arrangement is evaluated and designed in the Simulink environment. This parallel task intends to serve as a building block to scalable hybrid configurations that might require a more detailed nonlinear representation for a wide variety of controller schemes and hardware implementations.

Pray, hope, and don't worry. Do not worry over things that generate anxiety. Only one thing is necessary, to lift up your spirit and love God.

Padre Pio of Pietrelcina
1917

PREVIEW

*To my parents, Robert and Nellie Tsai, for the many blessings
bestowed on me through them.*

PREVIEW

Acknowledgements

This work is possible, thanks to the many combined prayers of family and friends, in particular those of my beloved mother, who probably hasn't slept in months. I am eternally grateful to my brother Scott for his constant intercession, my father for his patience and support, my baby girl for being my baby, and my wife Diana, for her care, love, and cooking that has kept me fat and healthy all these years. Without them, I would still be watching television going nowhere fast.

I would also like to thank my advisor Dr. Larry Banta, and the NETL team of Dr. David Tucker, Dr. John VanOsdol, Eric Liese, Larry Lawson, Susan Shoemaker, and David Rhuel. Special thanks go to my good friend Francesco Nicolo for his invaluable help and friendship. Funding for this research was provided by the National Energy Technology Laboratory.

Table of Contents

Abstract.....	ii
Acknowledgements.....	v
List of Figures	viii
Nomenclature.....	xii
1 Introduction.....	1
2 Literature Review.....	5
2.1 Solid Oxide Fuel Cell.....	5
2.2 The Brayton Cycle	9
2.3 Compressor Stall and Surge.....	11
2.4 Hybrid Configurations	14
2.5 Fuel Cell Models.....	29
2.6 Control Strategies and Designed Controllers.....	32
3 Method of Analysis.....	40
3.1 Hybrid Performance Facility Description.....	41
3.1.1 Auxiliary Power Unit.....	42
3.1.2 Primary Surface Recuperators	44
3.1.3 Combustor and Swift Valve.....	45
3.1.4 Air Plenum and Post Combustor.....	45
3.1.5 Bypass Valves	47
3.1.6 Instrumentation and Data Acquisition	49
3.2 Experimental Procedure	50
3.2.1 GAP Programming Sequence	50
3.2.2 Frequency Response Tests	51
3.3 Empirical Transfer Function Matrix	52
3.3.1 Transfer Function Generation.....	53
3.3.2 Multivariable Bode Plot and SVD	56
3.3.3 Relative Gain Array and MIMO Limitations.....	59
3.4 Robust H_{∞} Control Algorithm.....	60
3.4.1 Closed Loop Transfer Function Descriptions	60
3.4.2 Frequency Domain Specifications	62
3.4.3 H_{∞} Control Formulation.....	64
3.4.3.1 Mixed Sensitivity	65
3.4.3.2 Loop Gain Robustification.....	67
4 Empirical Results	73
4.1 Frequency Response Plots	73
4.2 Transfer Function Derivation.....	83
4.3 RGA and System Singular Values	93
4.4 Loop Gain Weight Selection.....	96
4.5 Controller Performance.....	100
4.5.1 Compensated Singular Values	100
4.5.2 Controller Implementation.....	102

4.5.3	Reference Tracking and Regulation.....	104
4.5.4	Uncertainty Analysis and Regulation	112
5	Analytical Model	115
5.1	Brayton Cycle	115
5.2	Balance of Plant	121
5.3	Compressor Model.....	125
5.4	Turbine Model	132
5.5	Air Plenum Model.....	135
5.5.1	Energy Conservation Equations: Plenum Control Volume	135
5.5.2	Energy Conservation Equation: Plenum Shell Control Volume....	137
5.6	Piping Model.....	140
5.6.1	Temperature Equation.....	140
5.6.2	Pressure Equation.....	147
5.7	Heat Exchanger Model	149
5.8	Combustor Model	156
5.9	Post Combustor Model	158
5.10	Bypass Valve Mass Flows	160
5.11	Fuel Valve Logic.....	161
5.11.1	Open Loop Command.....	162
5.11.2	Closed Loop Command	162
5.12	Analytical Model Results.....	163
5.12.1	Ramp Rate Startup Tests.....	163
5.12.2	Bypass Valve Simulation.....	166
5.12.3	Electrical Load Simulation	169
6	Conclusions and Discussion	172
6.1	Multivariate Transfer Function Matrix	172
6.2	Nonlinear Analytical Model	178
7	Future Work	181
	Bibliography	184
	Appendix A	190
	Appendix B	191
	Appendix C	193
	Appendix D.....	195
	Appendix E	196
	Appendix F.....	233
	Appendix G	235
	Appendix H.....	270
	Appendix I	272

List of Figures

Figure 2.1 SOFC Operation	6
Figure 2.1 Brayton Cycle Schematic (Saad 1997).....	9
Figure.2.3. Regenerative Brayton Cycle with Stage Compression (Saad 1997)	10
Figure.2.4. Simulated and Observed Results for the 220kW System [NFCRC]	15
Figure.2.5. Siemens-Westinghouse 220kW Hybrid System [NFCRC]	16
Figure.2.6. Atmospheric Hybrid [Veyo].....	17
Figure.2.7. Pressurized Hybrid [Veyo]	17
Figure.2.8. Pressurized Intercooled Hybrid [Veyo].....	18
Figure.2.9. Turbo-Charged Hybrid [Veyo].....	18
Figure.2.10. Base Cycle Configuration [Rao]	20
Figure.2.11. Single SOFC-HAT Cycle [Rao]	21
Figure.2.12. Dual SOFC-HAT cycle [Rao]	21
Figure.2.13. Above: Recuperated SOFC Hybrid Cycle. Below: Hardware Simulation..	23
Figure 3.1 NETL HyPer Facility	41
Figure 3.2 AutoCAD Rendering of HyPer Hardware Facility, courtesy of NETL	42
Figure 3.3 Turbine/Compressor Assembly	43
Figure 3.4 AutoCAD Drawing of Turbine Scroll Insert	43
Figure 3.5 Heat Exchangers and Blower	44
Figure 3.6 AutoCAD Rendering of the Combustor Canister.....	45
Figure 3.7 FC Cathode Simulator Without Insulation	46
Figure 3.8 Post Combustor Without Insulation	46
Figure 3.9 AutoCAD Rendering of the Midsection Post Combustor	47
Figure 3.10 Cold Air and Bleed Air Bypass Valves	48
Figure 3.11 Hot Air Bypass Valve and Flow Paths	48
Figure 3.12 HyPer Control Panel.....	49
Figure 3.13 Simulink Sinusoid Subsystem	51
Figure 3.14 GAP MatLab Signal Blocks	51
Figure 3.15 Graphical Generation of Transfer Function	54
Figure 3.16 Singular Values of a Sample 2x2 TF matrix	58
Figure 3.17 Closed Loop Control System [Glad]	61
Figure 3.18 Sensitivity and Complementary Sensitivity Constraints [Lewis].....	63
Figure 3.19 Low and High Frequency SV Bounds [Lewis]	64
Figure 3.20 Generation of “z” variables from “u” and “w”.....	65
Figure 3.21 Closed Loop and Extended Transfer Functions [36].....	66
Figure 3.22 Simplified Desired Loop Gain Shape.....	70
Figure 4.1 Time Series: Fuel Valve Modulation @ 1Hz	74
Figure 4.2 Time Series of Fuel Valve Modulation @ 0.5Hz.....	74
Figure 4.3 Time Series: Fuel Valve Modulation @ 0.1Hz	75
Figure 4.4 Time Series: Fuel Valve Modulation @ 0.01Hz	75
Figure 4.5 Time Series: Fuel Valve Modulation @ 0.001Hz	76
Figure 4.6 Fuel Valve Modulation Bode Plots: \dot{m} , P_{FC} , T_{FC}	77

Figure 4.7 Fuel Valve Modulation Bode Plots: TIT, Ω	77
Figure 4.8 Load Bank Modulation Bode Plots: \dot{m} , P_{FC} , T_{FC}	78
Figure 4.9 Load Bank Modulation Bode Plots: TIT, Ω	78
Figure 4.10 Bleed Air Modulation Bode Plots: TIT, Ω , Stem.....	80
Figure 4.11 Bleed Air Modulation Bode Plots: \dot{m} , P_{FC} , T_{FC}	80
Figure 4.12 Cold Air Modulation Bode Plots: TIT, Ω , Stem	81
Figure 4.13 Cold Air Modulation Bode Plots: \dot{m} , P_{FC} , T_{FC}	81
Figure 4.14 Hot Air Modulation Bode Plots: TIT, Ω , Stem	82
Figure 4.15 Hot Air Modulation Bode Plots: \dot{m} , P_{FC} , T_{FC}	82
Figure 4.16 Generated and Test Data Bode Plots: Fuel Valve	86
Figure 4.17 Generated and Test Data Bode Plots: Load Bank	86
Figure 4.18 Generated and Test Data Bode Plots: Bleed Air Valve.....	87
Figure 4.19 Generated and Test Data Bode Plots: Cold Air Valve	87
Figure 4.20 Generated and Test Data Bode Plots: Hot Air Valve	88
Figure 4.21 Cold Air Bypass Open Loop Step Response.....	89
Figure 4.22 Hot Air Bypass Open Loop Step Response.....	90
Figure 4.23 Fuel Valve Open Loop Step Response.....	91
Figure 4.24 Relative Gain Array.....	94
Figure 4.25 Scaled and Unscaled Open Loop Singular Values	95
Figure 4.26 Open Loop Sensitivity Function.....	96
Figure 4.28 Compensated Loop Gain Singular Values	101
Figure 4.29 Compensated Sensitivity Function Singular Values	101
Figure 4.30 Compensated Complementary Sensitivity Function SV	102
Figure 4.31 Simulink Control Configuration.....	103
Figure 4.32 Signal Reference Tracking: Step Command	104
Figure 4.33 Control Signal: Simultaneous Step Tracking	105
Figure 4.34 Signal Tracking: \dot{m}_{FC}	105
Figure 4.35 Control Signal: \dot{m}_{FC} Tracking.....	106
Figure 4.36 Signal Tracking: Ω	106
Figure 4.37 Control Signal: Ω Tracking	107
Figure 4.38 Signal Tracking: TIT	107
Figure 4.39 Control Signal: TIT Tracking	108
Figure 4.40 Load Step Disturbance Attenuation.....	108
Figure 4.41 Control Signal: Load Disturbance	109
Figure 4.42 Heat Step Disturbance Attenuation	109
Figure 4.43 Control Signal: Heat Disturbance.....	110
Figure 4.44 Step Response to 10% Zero/Pole Parametric Uncertainty	113
Figure 5.1 Gas Turbine Brayton Cycle	116
Figure 5.2 Gas Turbine Simulink Model	117
Figure 5.3 Compressor Temperature Subsystem	117
Figure 5.4 Compressor Pressure Subsystem	118
Figure 5.5 Combustor Temperature Subsystem.....	119
Figure 5.6 Turbine Power Subsystem	120
Figure 5.7 Gas Turbine Components with Speed Feedback Control.....	121
Figure 5.8 PID Controller Subsystem.....	121
Figure 5.9 Simulink Nonlinear Model	122

Figure 5.10 Gas Turbine Simulink Model	125
Figure 5.11 Compressor Blades, Control Volume, and Infinitesimal Volume Element	126
Figure 5.12 Velocity polygons of a radial flow compressor [31]	128
Figure 5.13 Absolute velocities in terms of relative and rotor velocities [31]	129
Figure 5.14 Mass Flow Rate and Compressor Work Subsystem.....	131
Figure 5.15 Compressor Pressure Subsystem	132
Figure 5.16 Compressor Temperature Subsystem	132
Figure 5.18 Cross-Section of Air Plenum.....	138
Figure 5.19 Air Plenum Subsystem: Mass Conservation	139
Figure 5.20 Air Plenum Subsystem: Empirical Backpressure.....	139
Figure 5.21 Air Plenum Subsystem: Energy Conservation	139
Figure 5.22 Air Plenum Subsystem: Heat Flux and Convection Coefficient	140
Figure 5.23 Air Plenum Subsystem: Solid Shell Energy Conservation.....	140
Figure 5.24 Pipe Cross-Sectional Schematic	142
Figure 5.25 Pipe Element: Temperature and Pressure Subsystems	143
Figure 5.26 Temperature Equation Subsystem	144
Figure 5.27 Overall and Partial Heat Transfer Coefficient Subsystem	145
Figure 5.28 Convection Coefficient Subsystem	146
Figure 5.29 Pressure Major Losses in Straight Pipe	148
Figure 5.30 Friction Factor Subsystem.....	149
Figure 5.31 Minor Pressure Losses Subsystem: Le/D Case	149
Figure 5.32 Heat Exchanger Subsystem: Wall Balance	151
Figure 5.33 Heat Exchanger Subsystem: Heat Calculation	151
Figure 5.34 Heat Exchanger Subsystem: Cold Side Temperature Equation	151
Figure 5.35 Heat Exchanger Subsystem: Hot Side Temperature Equation	152
Figure 5.36 Heat Exchanger Subsystem: NTU Block	152
Figure 5.37 Heat Exchanger Subsystem: NTU Subsystem	153
Figure 5.38 NTU Effectiveness Equation.....	154
Figure 5.39 Heat Flux Calculation Logic	155
Figure 5.40 Combustor Block Diagram.....	157
Figure 5.41 Post Combustor Subsystem: Mass Conservation	159
Figure 5.42 Post Combustor Subsystem: Inlet Air Energy Conservation	159
Figure 5.43 Post Combustor Subsystem: Shell CV	160
Figure 5.44 Post Combustor Subsystem: Energy Equation	160
Figure 5.45 Bypass Valve Mass Flow Characteristics.....	161
Figure 5.46 Combustor Heat Input Logic	161
Figure 5.47 PID Controller Subsystem	162
Figure 5.48 PID Controller Subsystem Inner Works.....	163
Figure 5.49 Startup Profile: PID Controller in Model	164
Figure 5.50 Startup Profile PI Controller in Model	165
Figure 5.51 Startup Profile PI Controller in Model	165
Figure 5.52 Plenum Airflow Response to CA Step Increase: 25%	166
Figure 5.53 Plenum Temperature Response to CA Step Increase: 25%.....	167
Figure 5.54 Plenum Pressure Response to CA Step Increase: 25%	167
Figure 5.55 Turbine Speed Response to CA Step Increase: 25%	168
Figure 5.56 TIT Response to CA Step Increase: 25%	168

Figure 5.57 Plenum Airflow Response to BA and EL Steps: PID	169
Figure 5.58 Plenum Temp Response to BA and EL Steps: PID.....	170
Figure 5.59 Turbine Speed Response to BA and EL Steps.....	170
Figure 5.60 TIT Response to BA and EL Steps.....	171
Figure 5.61 Plenum Press Response to BA and EL Steps: PID.....	171
Figure 6.1 Actual HyPer PI Scheme	178

PREVIEW

Nomenclature

A	Area
AFR	Air to Fuel Ratio
APU	Auxiliary Power Unit
ATR	Advanced Transport Reactor
BA	Bleed Air Valve
C	Capacitance
CA	Cold Air Valve
COE	Cost of Electricity
d	Diameter
e	Intensive Energy
EGT	Exhaust Gas Temperature
EL	Electrical Load
f	Friction Factor
FRR	Fuel Reformate Ratio
FU	Fuel Utilization
g	Constant of Gravity
GAP	Graphical
GAP	Graphical Application Programmer
GT	Gas Turbine
H	Angular Momentum
h	Enthalpy
H_∞	Hardy Space Infinity Norm
HA	Hot Air Valve
HAT	Humid Air Turbine
HHV	Higher Heating Value
HP,LP	High and Low Pressure
HX	Heat Exchanger
HyPer	Hybrid Performance
k	Conduction Coefficient
K	Loss Coefficient
k	PID Gain
Le	Equivalent Length
LHV	Lower Heating Value
LQG	Linear Quadratic Gaussian
LQR	Linear Quadratic Regulator
LTI	Linear Time Invariant
MIMO	Multiple Input Multiple Output
N	Rotational Shaft Speed
NETL	National Energy Technology Laboratory
NFCRC	National Fuel Cell Research Center
NTU	Number of Transfer Units
P	Pressure

PEM	Proton Exchange Membrane
PID	Proportional Integral Derivative
PR	Pressure Ratio
R	Universal Gas Constant
Re	Reynolds Number
RGA	Relative Gain Array
RHP	Right Hand Plane
Rt	Thermal Resistance
SISO	Single Input Single Output
SOFC	Solid Oxide Fuel Cell
STCR	Steam to Carbon Ratio
SVD	Singular Value Decomposition
T	Temperature
TF	Transfer Function
TIT	Turbine Inlet Temperature
u	Internal Energy
U	Overall Heat Transfer Coefficient
v	Velocity
V	Volume
W	Weight Matrix
YSZ	Yttria-Stabilized Zirconia
τ	Time Constant

Subscripts

amb	Ambient
BW	Bandwidth
comp	Compressor
CS	Control Surface
CV	Control Volume
d	Delay
l	Major Pressure Loss
lm	Minor Pressure Loss
n	Noise Bound
p	Plant
P	Pressure
ss	Steady State
st	Stored
surf	Surface

Symbols

ϵ	Effectiveness
ε	Relative Roughness
η	Efficiency
κ	Condition Number

μ	Dynamic Viscosity
ν	Kinematic Viscosity
ρ	Density
ω	Frequency

PREVIEW

1 Introduction

Fuel cell technology has fast advanced in the field of power generation, and is currently sought as one viable alternative for the replacement of conventional power systems, as an efficient and clean source of electricity. As the research in this field progresses, it is more evident that existing technologies must be incorporated in the design of these systems in order to achieve the highest possible efficiency without sacrificing performance or cost. It is therefore convenient to utilize the synergy of current power producing methods with power generating fuel cells. However, the resulting coupling difficulties of fuel cells and gas turbines are yet to be successfully mastered.

One of the most promising technologies for hybrid power generation systems is the coupling between Solid Oxide Fuel Cells and gas turbines. Siemens-Westinghouse and the National Fuel Cell Research Center or NFCRC for example, have recently built and tested one such system, capable of producing 220kW of power with more than 50% electrical efficiency based on the LHV of natural gas fuel. It is estimated that enhanced configurations of similar types of hybrid systems can deliver more than 70% efficiencies. This is far greater than systems running on coal or natural gas alone, for equivalent sized plants. In addition, fuel cells may offer advantages over conventional power plants in the area of carbon sequestration.

Despite the success of the NFCRC in proving the practical implementation of the conceptual hybrid design, the resulting system was meant to serve only as a test bed for future designs. There are still many issues to address, before a fully integrated and functional configuration is ready for commercialization. One such concern is the ability to safely control the plant in the presence of disturbances, as defined by sudden load demands. An inherent difficulty of the fuel cell – gas turbine assembly, is that interactions between the high-pressure gas turbine flow and the fragile fuel cell material can lead to severe equipment damage, and malfunction. This constitutes the essential control problem of hybrid systems, to successfully regulate and follow load demands in a

system that exhibits a wide mismatch between component time constants, and large differences between their structural strengths.

Researchers have sought to find the solution to these problems mostly with the use of analytical models that are subsequently incorporated into various control methodologies. To date, hundreds of models have been based on the first principles of energy and mass conservation, and presented in various degrees of complexity, ranging from lumped parameter, to one and two-dimensional models. This limited form of characterization can be primarily attributed to the lack of any test facility large enough to faithfully duplicate the effects of a real hybrid plant. An experimental facility robust enough to test the operational limits was simply not available, and for most, cost prohibitive. Without an alternate way in which to physically model the system, the analytical models could not be validated, nor their accuracy measured.

In face of these challenges, the National Energy Technology Laboratory, or NETL has designed and constructed a test facility that allows for the simulation of a hybrid system, under a particular hybrid configuration. The facility simulates with hardware a 300kW Solid Oxide Fuel Cell coupled to a gas turbine. Hardware control of this system has been partially achieved for quasi-steady state scenarios. However, centralized control has yet to be implemented for transient occurrences and other quasi-steady state conditions.

The main objectives of this research are:

- To make use of the existing NETL hybrid facility for the generation and subsequent analysis of frequency response data useful for control development
- To derive a set of mathematical equations stemming from the aforementioned frequency response tests that more realistically predict the hybrid component interactions
- To develop and implement a control methodology based on the derived empirical multivariate model that can robustly regulate fuel cell and turbo-machinery critical parameters

A successful completion of these tasks will result in the following original contributions of this work, primarily:

- The availability of real frequency response data of a hybrid system as given in magnitude and phase Bode plots
- The derivation of empirical Transfer Functions never before obtained for a hardware hybrid configuration
- The design of a centralized state space robust controller for a hybrid system based entirely on an experimental model
- The validation of existing analytical multivariate models with the use of the empirical Transfer Function matrix

The scope of this work thus lays in the development of a centralized robust controller that can manage flow to maintain fuel cell operational constraints under multivariate transient disturbances. A robust controller is necessary for the safe and stable implementation of such a hybrid system. This is especially the case when detailed models are unattainable due to the complexity of the system itself, like that of a coupled gas turbine compressor assembly, or a system having combustion dynamics as it is in the present case. Robustness, as defined by the ability to sustain control in the presence of model uncertainty, is also preferred in a system required to dismiss low frequency perturbations. Random loss of electrical load is, for the most part, a real life low frequency occurrence. Such events could impose the possible destructive forces on a fuel cell, when they are not dealt with accordingly, because of the inevitable rise in turbine speed, and hence mass flow that accompanies a loss of electrical load. Thus, a controller that can mitigate both, high and low frequency phenomena is desired for the early stages of the hybrid design. Frequency domain loop shaping techniques are suitable to achieve these goals. System identification can provide empirical transfer functions for the linear window of fuel cell operation, while more insight into system coupling effects can be gained by examination of Bode plots. These transfer functions are in turn used in the design of an H_{∞} controller, which can be tested offline with a high fidelity model of the hybrid configuration.

Online testing of the resultant controller design will provide a means of quantifying the applicability of the abovementioned control methodology to new assemblies of the hybrid configuration. With the use of every available input, including electrical load, bypass valves and fuel, such a design can be accomplished with maximum thermal management capability under a stable envelope of operation for any system disturbance.

An analytical nonlinear model of the hardware facility at NETL has also been developed in the MatLab/Simulink environment. This model serves as a complementary tool to the aforementioned empirical analysis. Although originally intended to predict steady state behavior, ongoing work aims at incorporating full system dynamics to more accurately predict transient system behavior. Adjustment and tuning of the model is necessary if controller performance is to be evaluated prior to its real time implementation on the physical facility.

2 Literature Review

Hybrid power generating systems of the fuel cell type are mainly categorized according to the energy management strategy used. Whether the process is a recuperated heat process, a heat of compression configuration or a steam turbine bottoming cycle, the performance is generally based on the power produced per unit fuel consumed with respect to the lower heating value LHV of the fuel utilized. Following is a description of the existing and suggested hybrid configurations in literature as well as the different types of controllers being adapted to each assembly.

2.1 Solid Oxide Fuel Cell

Fuel cells have been described as replenishable batteries that operate continuously under a constant fuel supply. These electrochemical devices are able to produce power as a result of the ionic interaction between hydrogen and oxygen. A fuel cell thus has cathode and anode electrodes, an electrolyte, and conductive interconnections that allow for the transport of electrons through a resistive load from cathode to anode sides. In principle, hydrogen is supplied at the anode side and oxygen at the cathode side. The overall reaction in the fuel cell can be summarized as that of Eq.2.1.1, where electrons and heat are released as a consequence of the exothermic reaction.



Power electronics coupled to a resistive load can then convert this generated DC voltage to AC, when the fuel cell is used in stationary power generating applications.

For the most part, fuel cells are distinguished by the type of electrolyte used. The solid oxide fuel cell electrolyte has a Yttria-Stabilized Zirconia YSZ ceramic solid structure that allows ionic transport while remaining impermeable to electrons. The cathode and anode sides are composed of a mixture of ceramic and metals, mainly a Zirconia cermet that allows high temperatures and high electronic conductivity. The interconnects between cathode and anode sides are made of Lanthanum Chromite, a ceramic that can

increase conductivity when mixed with compatible alkaline materials (Larminie et al. 2003). These components combined together can withstand temperatures of up to 1000°C, and produce as much as 250MW of power, when assembled in compounding stacks (Carlson et al. 2004). It is because of these characteristics that the solid oxide fuel cell SOFC is the favorable candidate for large power applications.

A simplified schematic of the SOFC is shown in Figure 2.1. As noted earlier, electrons are expelled from the hydrogen molecules when the H₂ reacts with two oxygen anions to produce water and heat. The anode and cathode half reactions are accordingly:



A graph showing cell performance based on voltage/current density data is shown in Appendix A.

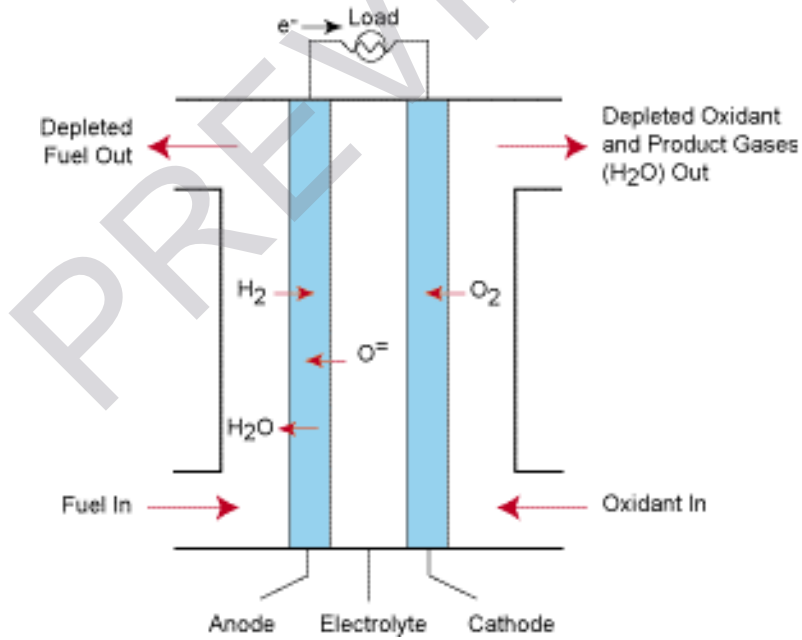


Figure 2.1 SOFC Operation

For this and any other fuel cell, the voltage produced is a function of the Gibbs free energy ΔG_f and thus of the reactant concentrations within the cell. The Gibbs free energy

is a measure of the amount of useable work that can be extracted from a chemical reaction. This energy is defined as the change in the enthalpy of formation minus the heat released as expressed in Eq.2.1.4. The fuel cell voltage can then be related to this available amount of work as that given by Eq.2.1.5.

$$\Delta g_f = \Delta h_f - T\Delta s \quad \text{Eq.2.1.4}$$

$$E_{OC} = -\frac{\Delta g_f}{z \cdot F} \quad \text{Eq.2.1.5}$$

where E_{OC} is the open circuit voltage, z is the number of electrons and F , Faraday's constant. In the presence of irreversibilities, the actual voltage per cell is given by the reversible Nernst potential cell voltage minus all irreversibilities, as shown in Eq.2.1.6,

$$E = E^0 + \frac{R \cdot T}{z \cdot F} \cdot \ln \left(\frac{\frac{P_{H_2}}{P^0} \cdot \left(\frac{P_{O_2}}{P^0} \right)^{\frac{1}{2}}}{\frac{P_{H_2O}}{P^0}} \right) - \eta_A - \eta_{FC} - \eta_O - \eta_C \quad \text{Eq.2.1.6}$$

$$E^0 = -\frac{\Delta h_f}{z \cdot F} \quad \text{Eq.2.1.7}$$

where the main irreversibilities η 's are those of activation, fuel crossover, ohmic, and concentration losses (Larminie et al. 2004). Equation 2.1.6 assumes that the oxidation process produces pure hydrogen to the cell. Activation losses are attributed to the voltage loss due to the driving force required to kick start the ionic exchange of the overall chemical reaction. Fuel crossover losses are those voltage drops observed when the electrolyte permits some electrons and fuel to permeate its membrane and mix with the cathode side stream. Ohmic losses are those relevant to the resistance of current flow, whereas concentration losses are those due to fluctuations in the stoichiometric quantities of the reactants. Ways in which to minimize these overpotentials are described in more detail in (Larminie et al. 2004). It can be seen from Eq.2.1.6 that the cell voltage is dependent on the partial pressures of the reactants, as well as the temperature of the cell.

Appendix A also shows how these irreversibilities affect the current voltage relationship in the cell.

So far it has been stated that fuel cells produce power by the electrochemical reaction of H₂ and O₂, once the latter is broken into anions. Hydrogen however, must be produced in pure form for the reaction to take place. With the use of pure H₂, power generation can result in zero pollutant emissions, having only water as a byproduct. Various methods to produce hydrogen exist, such as the use of primary fossil fuels like natural gas or coal. If coal is used, a gasification process combines high temperatures with water vapor and oxygen, while a natural gas fuel would require reforming and hydrogen shift reactions to produce H₂. Equations 2.1.8 and 2.1.9 detail the chemistry for the reforming, and shift reaction respectively of methane fuel (Karvountzi et al. 2004). Typical combustion NO_x and SO_x pollutants are thus eliminated in a fuel cell, having only the carbon dioxide capture logistics to handle.



Solid Oxide Fuel Cells are most suited to stationary hybrid power generation applications because they can operate at high enough temperatures to directly oxidize CO and CH₄. Proton Exchange Membrane fuel cells for example cannot withstand CO as a fuel or byproduct, because carbon monoxide poisons the electrolyte membrane. Since large realistic hybrid plants would require the production of massive amounts of hydrogen either by reforming a hydrocarbon or from coal syngas, it is likely that hydrocarbon byproducts appear at the anode along with hydrogen. The versatility of being able to withstand a wide variety of fuels, is a highly desirable feature of SOFC that becomes especially important if coal based systems are to be mandated.

In order for the fuel cell to maintain performance and operability, the cell's temperature, anode fuel flow, cathode airflow, and reactant partial pressure constraints must be met. Each of these parameters plays a major role in the thermal efficiency and the net power output of the fuel cell. Research on ways to optimize the cell's power production via the

synergistic use of its thermal characteristics has led to the successful coupling of existing gas turbine technology. In the following sections it will be seen that simple gas turbine cycles for stationary power generation benefit from exhausted fuel cell heat, while fuel cells increase in efficiency from recuperation and pressurized air, both byproducts of expanders and compressor assemblies.

2.2 The Brayton Cycle

A simple gas turbine cycle using air as the working fluid is illustrated in Fig.2.2. Ambient air enters point “1” and is adiabatically compressed to a higher temperature and pressure at point “2”. Heat through a combustor further increases the temperature of the compressed air at point “3”, where it is then expanded in a turbine to generate electrical power through a generator at point “4”. The ideal cycle for this configuration is known as the Brayton Cycle, and the closed loop version is shown to the right in Fig.2.2.

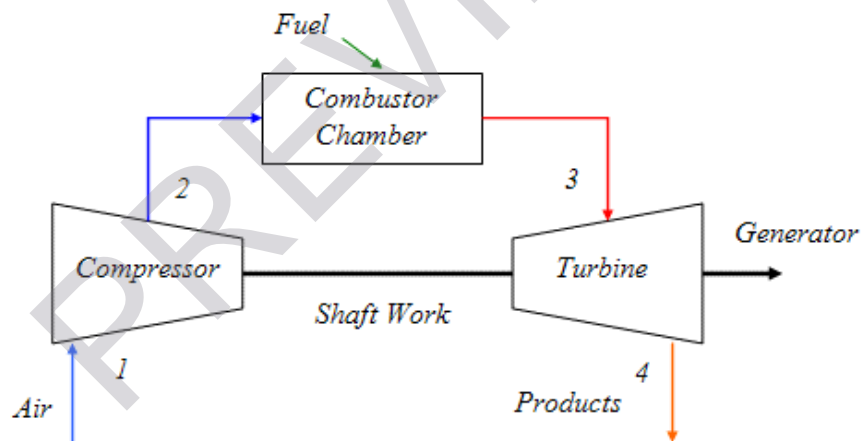


Figure 2.1 Brayton Cycle Schematic (Saad 1997)